Small Obstacle in a Large Polar Flock

Joan Codina,[1,2] Benoît Mahault,[3] Hugues Chaté,[4,5,6] Jure Dobnikar,[2,7,8]
Ignacio Pagonabarraga,[9,10,11] and Xia-qing Shi[12]

[1]*Wenzhou Institute, University of Chinese Academy of Sciences, Wenzhou 325001, China*
[2]*Key Laboratory of Soft Matter Physics, Institute of Physics, Chinese Academy of Sciences, Beijing 100190, China*
[3]*Max Planck Institute for Dynamics and Self-Organization (MPIDS), 37077 Göttingen, Germany*
[4]*Service de Physique de l'Etat Condensé, CEA, CNRS Université Paris-Saclay, CEA-Saclay, 91191 Gif-sur-Yvette, France*
[5]*Computational Science Research Center, Beijing 100193, China*
[6]*Sorbonne Université, CNRS UMR7600, Laboratoire de Physique Théorique de la Matière Condensée, 75005 Paris, France*
[7]*School of Physical Sciences, University of Chinese Academy of Sciences, Beijing 100049, China*
[8]*Songshan Lake Materials Laboratory, Dongguan, Guangdong 523808, China*
[9]*Departament de Física de la Matèria Condensada, Universitat de Barcelona, 08028 Barcelona, Spain*
[10]*Universitat de Barcelona Institute of Complex Systems, 08028 Barcelona, Spain*
[11]*Centre Européen de Calcul Atomique et Moléculaire, Ecole Polytechnique Fédérale de Lausanne, 1015 Lausanne, Switzerland*
[12]*Center for Soft Condensed Matter Physics and Interdisciplinary Research, Soochow University, Suzhou 215006, China*

(Received 16 December 2021; accepted 3 May 2022; published 23 May 2022)

We show that arbitrarily large polar flocks are susceptible to the presence of a single small obstacle. In a wide region of parameter space, the obstacle triggers counterpropagating dense bands leading to reversals of the flow. In very large systems, these bands interact, yielding a never-ending chaotic dynamics that constitutes a new disordered phase of the system. While most of these results were obtained using simulations of aligning self-propelled particles, we find similar phenomena at the continuous level, not when considering the basic Toner-Tu hydrodynamic theory, but in simulations of truncations of the relevant Boltzmann equation.

DOI: 10.1103/PhysRevLett.128.218001

In numerical and theoretical studies of active matter, polar flocks continue to play a central role (see, e.g., [1–13] for recent examples). This term refers to the homogeneous collective motion, resulting from spontaneous rotational symmetry breaking, of self-propelled particles locally aligning their velocities, as in the Vicsek model [14–16]. Remarkably, polar flocks exhibit true long-range polar order even in two space dimensions (2D), as argued by Toner and Tu, who also predicted the scaling structure of their space-time fluctuations [5,17–19]. Since these early works, a wealth of results have been obtained on particle-level models, hydrodynamic theories, and even experimental realizations of polar flocks [20–25]. The overall phase diagram of such dry aligning dilute active matter is best described as resulting from a phase-separation scenario in which homogeneous polar flocks form an orientationally ordered liquid separated from a disordered gas by a coexistence phase involving dense and ordered traveling bands [16,26,27]. This has been recently shown to hold even in the case of nonmetric, "topological" interactions, a case that was heretofore believed to show a direct order-disorder transition [9].

Polar flocks are thus observed in a rather large class of active matter systems and there is evidence of the robustness of their properties. But there are also clear indications of their fragility. For instance even weakly nonreciprocal interactions have been shown to substantially modify phase diagrams [7,28,29] (see also [30,31]). Further evidence is found in recent works that demonstrated a variety of effects induced by spatially distributed quenched disorder [13,32–36]. The Toner-Tu long-range polar order has been argued to be qualitatively changed for flocks moving on disordered substrates. It has been shown that different types of quenched disorder can have different effects. In most cases, arbitrarily weak distributed disorder modifies or breaks long-range polar order.

The above cases of quenched disorder include that of many scattered small obstacles, which was considered in models and in experiments [32,35]. But what about the effect of a single obstacle? The insertion of a passive object in a disordered gas of active particles is known to have nontrivial consequences, introducing in particular long-range currents in the active gas [37–43]. Given this, one can expect that even a single passive obstacle introduced within a long-range correlated polar flock may have major consequences on the large-scale dynamics of the system.

In this Letter, we explore the consequences of the introduction of a single fixed obstacle in the flow exhibited by 2D polar flocks using both self-propelled particles models and continuous theories. We show that, in a large

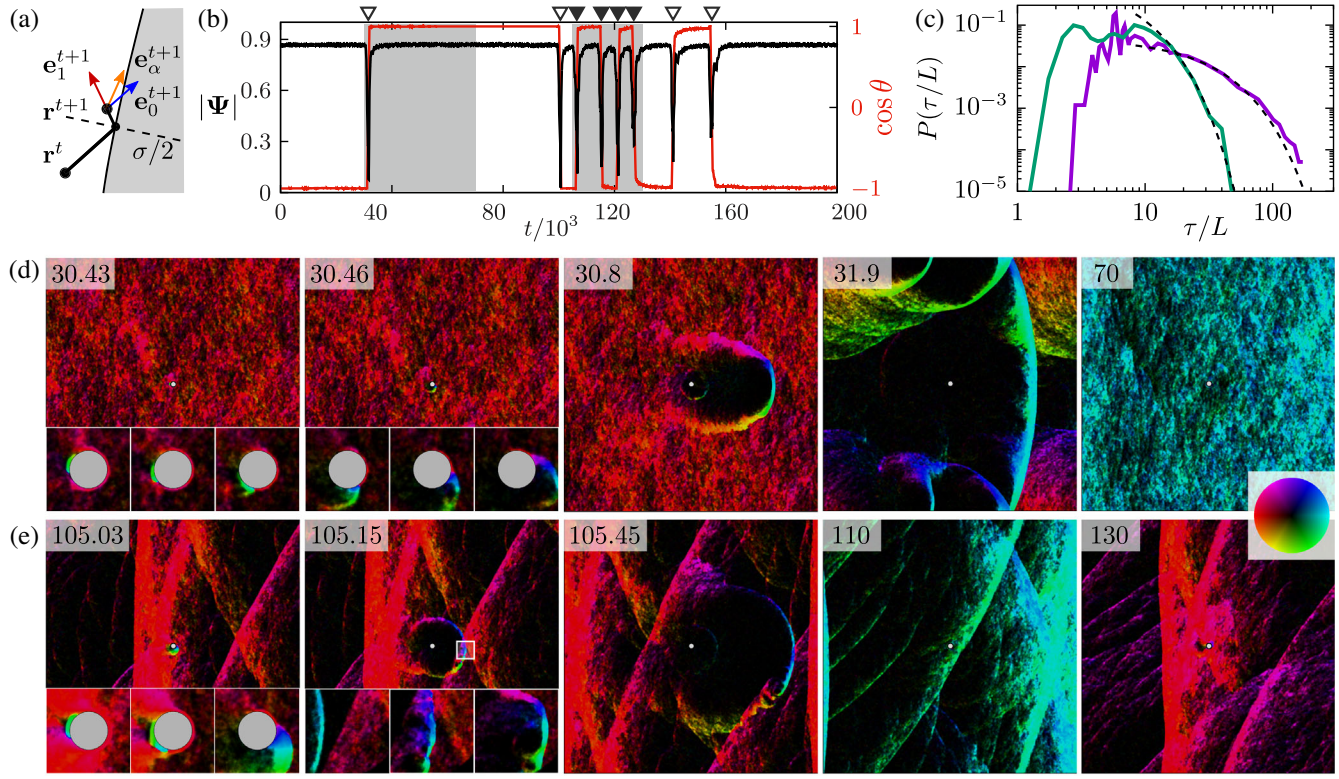

FIG. 1. Typical flow reversals ($\eta = 0.5$, $L = 1024$). (a) Sketch of collision rules: postcollision orientation $\boldsymbol{e}_\alpha^{t+1}$ interpolates between the precollision one ($\alpha = 0$, blue arrow) and that of the reflected trajectory ($\alpha = 1$, red arrow). (b) Time series of the global polarization $|\boldsymbol{\Psi}|$, in black, and its orientation $\cos\theta$, in red; shaded regions indicate the time windows for the snapshots series in (d), and (e); the empty and filled triangles indicate reversals triggered respectively from the homogeneous flock state [such as in (d)] and from the passage of a dense band (such as in (e) ($\alpha = 0, \sigma = 22$). (c) Distributions of inter-reversal times $P(\tau)$; dashed lines indicate exponential decays (green line: $\alpha = 0, \sigma = 22$; purple line: $\alpha = 0.325, \sigma = 120$). (d),(e) Snapshots of the system shown in (b) during an isolated reversal (d), and a reversal triggered by the passage of the dense band (e). On the color wheel on the right, color and intensity represent, respectively, the angle of the locally averaged polarity and the locally averaged density (with black for near-empty regions). The obstacle (at the center of the images) is in gray. Time marks are indicated at the top of each panel in units of 1000 time steps. For the first 2 panels, enlargements are provided showing the birth of the counterpropagating front around the obstacle. See Movies S1–S4 and S1z–S2z in [45].

part of the ordered liquid phase, even a small disk can reverse the global orientation of very large flocks. Such reversals occur via the nucleation, ballistic invasion, and complex interactions of counterpropagating dense bands. For very large systems, reversals become complex events of increasing duration, and we conjecture that asymptotically the flock never repairs itself. Our data indicate that orientational order is fully broken and self-averages in the infinite-size limit, albeit with very large correlation scales. At the continuous level, we find that the standard Toner-Tu hydrodynamic theory is unable to account for these phenomena, something low-order truncations of the Boltzmann equation for polar flocks can do.

In most of this work, we make use of a standard 2D Vicsek model with vectorial noise [44]: point particles $i = 1, 2, \ldots, N$, with positions $\boldsymbol{r}_i$ and unit orientations $\boldsymbol{e}_i$ move at constant speed v_0 in discrete time steps:

$$\boldsymbol{r}_i^{t+1} = \boldsymbol{r}_i^t + v_0 \boldsymbol{e}_i^{t+1}, \tag{1a}$$

$$\boldsymbol{e}_i^{t+1} = \vartheta[\langle \boldsymbol{e}_j^t \rangle_{j\sim i} + \eta \boldsymbol{\xi}], \tag{1b}$$

where ϑ normalizes vectors ($\vartheta(\boldsymbol{u}) = \boldsymbol{u}/\|\boldsymbol{u}\|$), the average is taken over all particles j within unit distance of i including i, and $\boldsymbol{\xi}$ is a random-orientation unit vector drawn independently for each particle at each time step. This may seem an odd choice for modeling collisions with an obstacle since particles have no physical size, and discrete-time dynamics look inconvenient. Our motivation here, though, is to be able to reach the asymptotic regime of polar flocks, which is known to require very large system sizes, even for Vicsek-like systems [5], and remains inaccessible with more realistic particles.

In this Vicsek context, collisions with an obstacle can be implemented in various ways. We have considered a one-parameter family of collision rules (cf. Fig. 1(a), with more details in [45]). Colliding particles are those whose next position is calculated to land inside the obstacle. Their postcollision location $\boldsymbol{r}_i^{t+1}$ is given by a simple reflection on

the obstacle surface. Their postcollision orientation $\boldsymbol{e}_i^{t+1}$ interpolates, via parameter α, between that given by the reflected trajectory ($\alpha = 1$) and the precollision orientation ($\alpha = 0$). This last case is reminiscent of the collision dynamics observed between hard metallic disks endowed with a built-in polar axis (see, e.g., [20,21]). On the other hand, the alignment of orientation along the reflected path ($\alpha = 1$) is akin to the classic description of a gas of passive point particles. The phenomena reported below were observed with $0 \leq \alpha < \frac{1}{2}$.

We consider a single fixed circular obstacle of diameter σ in a square domain of linear size L with periodic boundary conditions. For simplicity, we set the global density $\rho_0 = N/L^2 = 2$ and $v_0 = 1$. The pure, obstacleless system exhibits the 3 expected phases as the noise strength η decreases: a disordered gas for $\eta \gtrsim 0.65$, the homogeneous Toner-Tu polar flock phase for $\eta \lesssim 0.56$, and the coexistence phase with its signature traveling bands in between. Here, we are mostly concerned with the polar flock phase.

Monitoring the global order parameter $\boldsymbol{\Psi} = \langle \boldsymbol{e}_i \rangle_i$, we observe, at $\alpha = 0$, that a large-enough obstacle triggers sudden changes in $\theta = \arg \boldsymbol{\Psi}$, the global flow direction, accompanied by sharp dips of $|\boldsymbol{\Psi}|$ [Fig. 1(b)]. Most of these events are full reversals during which θ changes by π [46]. Reversals are also observed for $0 < \alpha < \frac{1}{2}$, but the minimal obstacle size needed to trigger them, which is of the order of 10 for $\alpha = 0$, increases with α and seems to diverge when $\alpha \to \frac{1}{2}$ [45].

In the regime shown in Fig. 1, we in fact observe two types of reversals marked by open and filled triangles in Fig. 1(b). The first type of reversal is triggered by the obstacle when the system has returned to the homogeneous steady state: a dense blob of counterpropagating particles is nucleated at the rear of the obstacle. It then recruits more and more particles as it moves along and detaches from the obstacle, forming a dense, curved band that invades the whole system ballistically. In the final stage, the global polarity is now typically reversed, and this band, which has now connected itself across the periodic boundaries, widens slowly (Fig. 1(d), and Movies S1, S1z, and S3 in [45]). This slow recovery can proceed until the homogeneous steady state is recovered, but it can also be interrupted at the occasion of one of the multiple passages of the band "through" the obstacle. As shown in Fig. 1(e) and Movies S2, S2z, and S4 in [45], a passing band can trigger a new counterpropagating dense front that can reverse (again) the global polarity. This constitutes our second type of reversal.

Note that the initial stages leading to a reversal are common to both types of reversals [compare the insets of Figs. 1(d) and 1(e)]: with sufficiently small α, the polarity of colliding particles persists and they glide along the obstacle, meeting at the rear where they align and accumulate, possibly forming the dense-enough blob that can then glide back on one side of the obstacle and eventually detach.

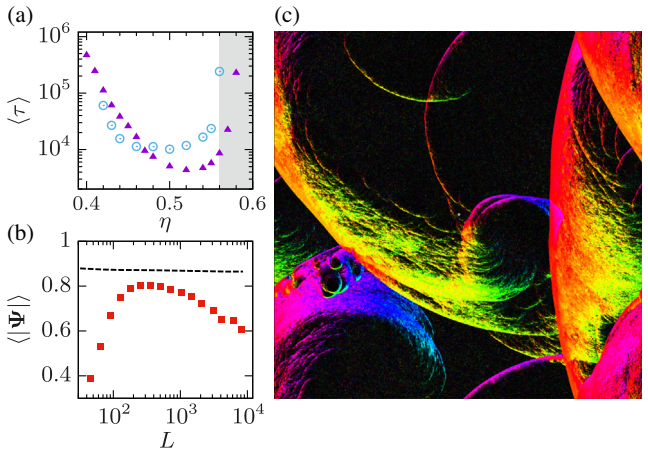

FIG. 2. (a) Average inter-reversal time, $\langle \tau \rangle$ vs η (purple triangles $\alpha = 0$, $\sigma = 35$, $L = 256$; blue circles $\alpha = 0.325$, $\sigma = 120$, $L = 1024$); the shaded region indicated the band phase of the pure system. (b) Average global polarization vs system size with obstacle (red squares) and without (dashed line) ($\alpha = 0$, $\eta = 0.5$, $\sigma = 35$). (c) Snapshot of a $L = 4096$ system [$\alpha = 0$, $\eta = 0.5$, $\sigma = 35$, colors as in Fig. 1(a)]; at these parameters the system almost never recovers the homogeneous polar state. See related Movie S5 in [45].

Because they are preceded by slow recoveries of the homogeneous polar liquid, first-type reversals statistics are described by the tail of the distribution of inter-reversal times τ, which we found exponential indicating independent nucleationlike events [Fig. 1(c)]. Conversely, the second-type reversals are correlated, resulting in nonexponential behavior at smaller τ (sometimes regimes with almost periodic second-type reversals are observed). For the parameters used in Fig. 1, the first-type reversals are dominating. However, the relative frequency of the two types of reversals varies with parameters and system size in a complicated manner [47]. In all cases, though, we observe the same behavior for the variation of $\langle \tau \rangle$ with the noise strength η: $\langle \tau \rangle$ takes a minimal value near $\eta \simeq 0.5$ and increases very fast both when decreasing η from this value and when approaching the boundary of the coexistence band phase (Fig. 2(a), note the log scale). The existence of a minimum of $\langle \tau \rangle(\eta)$ can be rationalized as follows: decreasing η, the homogeneous flock phase (and the incoming bands, in the case of the second type of reversal) is more and more stable, making it harder for the nucleated counterpropagating dense group to win. On the other side, approaching the coexistence phase, there are stronger fluctuations in the incoming flow, which lowers the probability of forming an initial counterpropagating group.

All results shown so far have been obtained with system sizes L much larger than the obstacle diameter σ, and it is thus clear that a small object can frequently reverse the global order of even a large flock. But in cases such as that presented in Fig. 1, the time-averaged order parameter $\langle |\boldsymbol{\Psi}| \rangle_t$ keeps a fairly large value in spite of reversals,

essentially because they remain rather well-separated events. However, simulating much larger systems reveals that the ballistic expansion of the counterpropagating band typically does not lead to simple "reconnection" across the boundaries as it does in Fig. 1(d). Instead, the system can engage in a long, complicated process during which bands cross, or meet the obstacle, leading to the nucleation of more bands (Fig. 2(c) and Movie S5 in [45]). One cannot distinguish reversals anymore and the global dynamics becomes chaotic as the system size is increased. Consequently, $\langle|\mathbf{\Psi}|\rangle_t$ decreases with increasing L, approaching the scaling of a self-averaging disordered phase [Fig. 2(b)]. Extrapolating these results, we conclude that a single obstacle asymptotically destroys order. Data such as those in Fig. 2(b) could only be obtained for "favorable" η values near 0.5, where, at moderate system size, $\langle\tau\rangle$ is not too large. We nevertheless believe global order is asymptotically destroyed over the larger range of noise strengths where we are able to observe reversals. This range, however, remains fairly limited.

Reversals due to the presence of an obstacle become exceedingly rare when decreasing η. To probe whether they can be triggered at low noise strengths, we study the fate of polar flocks in which we artificially introduce a dense blob of particles orientated against the main flow (details in [45]), and watch the subsequent evolution. (Note that such a blob mimics what happens spontaneously at the rear of the obstacle.) We limit ourselves to circular blobs of diameter σ_b and density ρ_b, and work with system sizes much larger than σ_b for which the number of particles in the blob remains much smaller than N. In the range of η values where we can observe reversals triggered by an obstacle, a large-enough and dense-enough blob reverses the initial flow. These blob-induced reversals are similar to obstacle-induced ones, the main difference being that the blob vanishes completely after its introduction. As η is decreased, though, a given blob does not always lead to a reversal (see Movie S6 in [45]). We find that P_{rev}, the probability to reverse the flow upon the introduction of a given blob, varies from 0 to 1 when η is increased, in a manner consistent with a hyperbolic tangent [Fig. 3(a)]. This allows to define a transitional value η^* (at $P_{\mathrm{rev}} = \frac{1}{2}$), and to see how it varies with ρ_b and σ_b. As expected, this procedure works not only for the η values "accessible" with a fixed obstacle, but also with smaller values. However, as shown in Fig. 3(b), we identify a minimal value $\eta \simeq 0.40$ below which no blob, however dense, triggers a reversal. This suggests that only a fraction of the Toner-Tu phase is destroyed by a single localized obstacle.

We finally explore whether continuous kinetic or hydrodynamic theories of polar flocks can also account for the phenomena reported above. For numerical convenience, we did not consider a fixed obstacle but only studied the fate of an initial small circular blob oriented against the main order. Remarkably, when using standard hydrodynamic

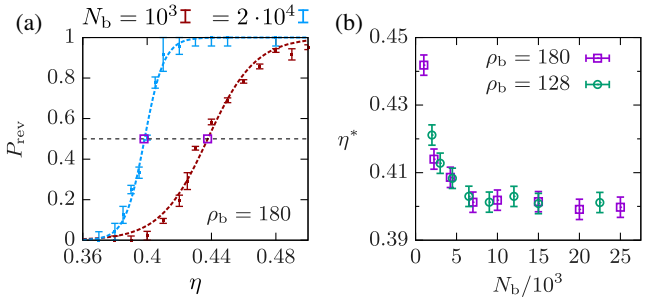

FIG. 3. Reversals triggered by the introduction of a finite blob of counterpropagating particles ($L = 1024$). (a) Reversal probability P_{rev} vs η at different N_b for $\rho_b = 180$, magenta squares indicate the estimated value for η^*. (b) η^* for different ρ_b as a function of the number of particles in the blob N_b.

Toner-Tu equations [45] no blob, however dense, seems able to trigger a growing counterpropagating band (and thus a reversal) anywhere in the ordered phase. The initial blob splits into two wings that "diffuse away" (not shown). On the other hand, reversals do occur when considering low-level truncations of the Boltzmann equation for the Vicsek or polar class. This equation has been introduced elsewhere and mostly used to derive hydrodynamic theories [27,48–50]. Here we only provide a sketch, with all details given in [45]. The Boltzmann equation governs the one-body probability distribution function $f(\boldsymbol{r}, \theta, t)$ of finding a particle with velocity orientation θ at position $\boldsymbol{r}$ and time t:

$$\partial_t f + v_0 \boldsymbol{e}(\theta) \cdot \nabla f = I_{\mathrm{sd}}[f] + I_{\mathrm{co}}[f], \tag{2}$$

where $\boldsymbol{e}(\theta)$ is the unit vector along θ, and I_{sd} and I_{co} are self-diffusion and collision integrals. Expanding f in angular Fourier modes $f(\boldsymbol{r}, \theta, t) = \frac{1}{2\pi} \sum_k f_k(\boldsymbol{r}, t) \exp(-ik\theta)$, the Boltzmann equation is turned into a hierarchy of coupled partial differential equations for the complex fields f_k:

$$\partial_t f_k + \frac{1}{2}(\nabla^* f_{k+1} + \nabla f_{k-1}) = \alpha_k f_k + \sum_q J_{k,q} f_q f_{k-q}, \tag{3}$$

where $\nabla = \partial_x + i\partial_y$, and α_k and $J_{k,q}$ are coefficients depending on parameters given in [45]. The Toner-Tu hydrodynamic theory is recovered when truncating and closing [Eq. (3)] using a scaling ansatz that essentially sets all $f_{k>2} = 0$, and enslaves f_2, the nematic order field, to the polar field f_1. Here, after realizing that this theory cannot account for reversals, we considered abrupt truncations of Eq. (3) at order K, simply setting $f_{k>K} = 0$ and integrating the remaining set of $K + 1$ equations (for numerical details, see [45]).

The lowest order K at which we could observe a full reversal is $K = 4$ [51]. Figure 4(a) shows snapshots of the evolution of an initial blob in this case (see also Movie S7 in [45]), which is remarkably similar to that observed with the Vicsek model. That our set of equations is able to

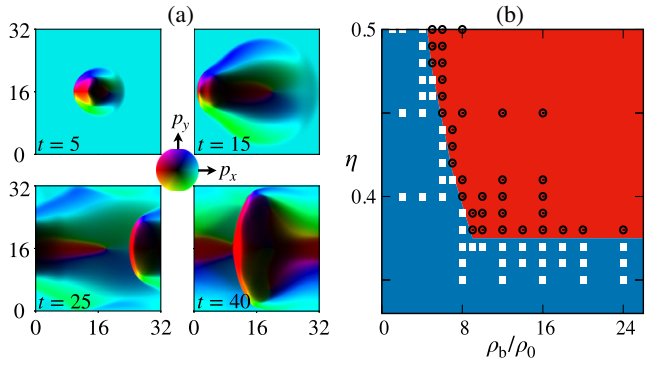

FIG. 4. Simulations of the Boltzmann equation [Eq. (3)] truncated at $K = 4$ at system density $\rho_0 = 2$ and blob radius $\sigma_b = 2$. (a) Snapshots showing the evolution of the momentum field ($f_1 = p_x + ip_y$) at noise $\eta = 0.5$ after introduction of a blob with density $\rho_b = 8\rho_0$ in the ordered solution at time $t = 0$. Note that the bivariate color map leads dilute disordered regions to appear darker. (b) Fate of blob in the (ρ_b, η) plane: black circles mark parameters leading to a reversal, while white squares indicate where no reversal occurs. More details about the numerical protocol in [45].

reproduce the development of a reversal is testimony that this dynamics is essentially deterministic. This allows us to scan parameter space systematically using single runs. In Fig. 4(b) we show the result of such an exploration in the (η, ρ_b) plane. We find an abrupt limit in η below which no blob can lead to a reversal (see Movie S7 in [45]), again in agreement with the microscopic-level results shown in Fig. 3(b).

To summarize, we have shown that arbitrarily large polar flocks are susceptible to the presence of a single small obstacle: In a fairly wide region of the ordered Toner-Tu phase, the obstacle triggers counterpropagating dense bands leading to reversals of the flow. We observed reversals at the microscopic level, but also in truncations of the relevant Boltzmann equation. This stresses the genericity of reversals. However, we were unable to observe them within the standard Toner-Tu hydrodynamic theory. This may be a manifestation of the limitations of simple hydrodynamic theories to account for highly nonlinear spatiotemporal dynamics (see [52] for a similar observation in the context of active nematics).

In very large systems we observe complex chaotic dynamics where the band triggered initially leads to other bands when passing the obstacle. These bands interact among themselves, creating new ones (Movie S5), leading to global disorder asymptotically. As a matter of fact, one can wonder, since bands interact and multiply between themselves, whether the chaotic dynamics observed could be sustained even in the absence of the obstacle. At the sizes explored here, the system eventually recovers from the band chaos created by an initial blob, so that the answer to this important question is so far unknown, but certainly worth exploring further.

We thank Yu Duan and Yongfeng Zhao for useful comments. We acknowledge generous allocations of CPU time on the Living Matter Department cluster in MPIDS, and on Beijing CSRCs Tianhe supercomputer. The work was supported by the EUs Horizon 2020 Program (Grant No. FET-OPEN 766972-NANOPHLOW to J. D. and I. P.), the French ANR through the project NeqFluids (Grant No. ANR-18-CE92-0019 to H. C.), the National Natural Science Foundation of China (Grants No. 11635002 to X.-q. S. and H. C., 11922506 and 11674236 to X.-q. S., 11874398 and 12034019 to J. D.), the Strategic Priority Research Program of the Chinese Academy of Sciences (Grant No. XDB33000000 to J. D.), and an international collaboration grant from the K. C. Wong Education Foundation (to J. D.). I. P. acknowledges support from Ministerio de Ciencia, Innovación y Universidades MCIU/AEI/FEDER (Grant No. PGC2018-098373-B-100 AEI/FEDER-EU), Generalitat de Catalunya (Project No. 2017SGR-884), and the Swiss National Science Foundation (Project No. 200021-175719).

[1] A. Souslov, B. C. van Zuiden, D. Bartolo, and V. Vitelli, Nat. Phys. **13**, 1091 (2017).
[2] A. Martín-Gómez, D. Levis, A. Díaz-Guilera, and I. Pagonabarraga, Soft Matter **14**, 2610 (2018).
[3] M. Kourbane-Houssene, C. Erignoux, T. Bodineau, and J. Tailleur, Phys. Rev. Lett. **120**, 268003 (2018).
[4] D. Geyer, D. Martin, J. Tailleur, and D. Bartolo, Phys. Rev. X **9**, 031043 (2019).
[5] B. Mahault, F. Ginelli, and H. Chaté, Phys. Rev. Lett. **123**, 218001 (2019).
[6] K. Sone and Y. Ashida, Phys. Rev. Lett. **123**, 205502 (2019).
[7] L. P. Dadhichi, J. Kethapelli, R. Chajwa, S. Ramaswamy, and A. Maitra, Phys. Rev. E **101**, 052601 (2020).
[8] H. Tasaki, Phys. Rev. Lett. **125**, 220601 (2020).
[9] D. Martin, H. Chaté, C. Nardini, A. Solon, J. Tailleur, and F. Van Wijland, Phys. Rev. Lett. **126**, 148001 (2021).
[10] M. James, D. A. Suchla, J. Dunkel, and M. Wilczek, Nat. Commun. **12**, 5630 (2021).
[11] E. Sesé-Sansa, D. Levis, and I. Pagonabarraga, Phys. Rev. E **104**, 054611 (2021).
[12] Y. Zhao, T. Ihle, Z. Han, C. Huepe, and P. Romanczuk, Phys. Rev. E **104**, 044605 (2021).
[13] Y. Duan, B. Mahault, Y.-q. Ma, X.-q. Shi, and H. Chaté, Phys. Rev. Lett. **126**, 178001 (2021).
[14] T. Vicsek, A. Czirók, E. Ben-Jacob, I. Cohen, and O. Shochet, Phys. Rev. Lett. **75**, 1226 (1995).
[15] F. Ginelli, Eur. Phys. J. Special Topics **225**, 2099 (2016).
[16] H. Chaté, Annu. Rev. Condens. Matter Phys. **11**, 189 (2020).
[17] J. Toner and Y. Tu, Phys. Rev. Lett. **75**, 4326 (1995).
[18] J. Toner and Y. Tu, Phys. Rev. E **58**, 4828 (1998).
[19] J. Toner, Phys. Rev. E **86**, 031918 (2012).
[20] J. Deseigne, O. Dauchot, and H. Chaté, Phys. Rev. Lett. **105**, 098001 (2010).

[21] C. A. Weber, T. Hanke, J. Deseigne, S. Léonard, O. Dauchot, E. Frey, and H. Chaté, Phys. Rev. Lett. **110**, 208001 (2013).
[22] N. Kumar, H. Soni, S. Ramaswamy, and A. Sood, Nat. Commun. **5**, 4688 (2014).
[23] H. Soni, N. Kumar, J. Nambisan, R. K. Gupta, A. K. Sood, and S. Ramaswamy, Soft Matter **16**, 7210 (2020).
[24] D. Geyer, A. Morin, and D. Bartolo, Nat. Mater. **17**, 789 (2018).
[25] J. Iwasawa, D. Nishiguchi, and M. Sano, Phys. Rev. Research **3**, 043104 (2021).
[26] A. P. Solon, H. Chaté, and J. Tailleur, Phys. Rev. Lett. **114**, 068101 (2015).
[27] H. Chaté and B. Mahault, in *Active Matter and Non-Equilibrium Statistical Physics: A Synthetic and Self-Contained Overview*, edited by J. Tailleur (Oxford University Press, New York, 2021), Chap. Dilute Dry Aligning Active Matter.
[28] Q.-s. Chen, A. Patelli, H. Chaté, Y.-Q. Ma, and X.-Q. Shi, Phys. Rev. E **96**, 020601(R) (2017).
[29] M. Fruchart, R. Hanai, P. B. Littlewood, and V. Vitelli, Nature (London) **592**, 363 (2021).
[30] O. Chepizhko, D. Saintillan, and F. Peruani, Soft Matter **17**, 3113 (2021).
[31] R. Kürsten and T. Ihle, Phys. Rev. E **104**, 034604 (2021).
[32] O. Chepizhko, E. G. Altmann, and F. Peruani, Phys. Rev. Lett. **110**, 238101 (2013).
[33] J. Toner, N. Guttenberg, and Y. Tu, Phys. Rev. Lett. **121**, 248002 (2018).
[34] J. Toner, N. Guttenberg, and Y. Tu, Phys. Rev. E **98**, 062604 (2018).
[35] A. Chardac, S. Shankar, M. C. Marchetti, and D. Bartolo, Proc. Natl. Acad. Sci. U.S.A. **118**, 2018218118 (2021).
[36] P. Rahmani, F. Peruani, and P. Romanczuk, Commun. Phys. **4**, 206 (2021).
[37] Y. Baek, A. P. Solon, X. Xu, N. Nikola, and Y. Kafri, Phys. Rev. Lett. **120**, 058002 (2018).
[38] O. Granek, Y. Baek, Y. Kafri, and A. P. Solon, J. Stat. Mech. (2020) 063211.
[39] C. M. Rohwer, M. Kardar, and M. Krüger, J. Chem. Phys. **152**, 084109 (2020).
[40] M. Knežević and H. Stark, New J. Phys. **22**, 113025 (2020).
[41] P. Liu, S. Ye, F. Ye, K. Chen, and M. Yang, Phys. Rev. Lett. **124**, 158001 (2020).
[42] M. Sebtosheikh and A. Naji, Sci. Rep. **10**, 15570 (2020).
[43] T. Speck and A. Jayaram, Phys. Rev. Lett. **126**, 138002 (2021).
[44] G. Grégoire and H. Chaté, Phys. Rev. Lett. **92**, 025702 (2004).
[45] See Supplemental Material at http://link.aps.org/supplemental/10.1103/PhysRevLett.128.218001 for additional information on the modeling approaches and the descriptions of the supplemental movies (S1–S7).
[46] In rare cases, $\pm\frac{\pi}{2}$ rotations are observed.
[47] This complex situation will be detailed in a forthcoming publication.
[48] E. Bertin, M. Droz, and G. Grégoire, Phys. Rev. E **74**, 022101 (2006).
[49] E. Bertin, M. Droz, and G. Grégoire, J. Phys. A **42**, 445001 (2009).
[50] A. Peshkov, E. Bertin, F. Ginelli, and H. Chaté, Eur. Phys. J. Special Topics **223**, 1315 (2014).
[51] We also observed reversals using higher-order truncations, but the necessary numerical resolution is quickly prohibitively high.
[52] L.-b. Cai, H. Chaté, Y.-q. Ma, and X.-q. Shi, Phys. Rev. E **99**, 010601(R) (2019).